*J. Fluid Mech.* (1997), *vol.* 352, *pp.* 265–281. Printed in the United Kingdom



# Non-parallel linear stability analysis of the vertical boundary layer in a differentially heated cavity

By A. M. H. BROOKER[1]†, J. C. PATTERSON[1]‡ AND S. W. ARMFIELD[2]

[1]Centre for Water Research, The University of Western Australia, Nedlands 6907, Australia

[2]Department of Mechanical and Mechatronic Engineering, Sydney University, Sydney 2006, Australia

(Received 2 November 1995 and in revised form 23 July 1997)

A non-parallel linear stability analysis which utilizes the assumptions made in the parabolized stability equations is applied to the buoyancy-driven flow in a differentially heated cavity. Numerical integration of the complete Navier–Stokes and energy equations is used to validate the non-parallel theory by introducing an oscillatory heat input at the upstream end of the boundary layer. In this way the stability properties are obtained by analysing the evolution of the resulting disturbances. The solutions show that the spatial growth rate and wavenumber are highly dependent on the transverse location and the disturbance flow quantity under consideration. The local solution to the parabolized stability equations accurately predicts the wave properties observed in the direct simulation whereas conventional parallel stability analysis overpredicts the spatial amplification and the wavenumber.

## 1. Introduction

Buoyancy-driven flow in a side-heated cavity is the subject of continuing research. From the point of view of its engineering applications and fluid mechanical aspects the manner by which the flow is transformed from a steady laminar regime to an unsteady turbulent regime, as the Grashof number is increased, is of particular interest. The instability of the vertical boundary layers that are formed in a side-heated cavity is one of several mechanisms for the transformation to a turbulent flow.

Three distinctive flow regimes in which the boundary layer instability plays an important role in the transition to turbulence have been identified. The first is the steady boundary layer in an unstratified environment where travelling waves in the boundary layer are observed downstream of a critical height (see for example Szewczyk 1962 and Gebhart *et al.* 1988). The perturbations evolve from natural disturbances within the flow, are amplified as they travel downstream and eventually become turbulent. In Polymeropoulos & Gebhart (1967) this instability was studied experimentally by artificially introducing disturbances of particular frequencies into the flow. The second regime is the occurrence of amplifying wave packets in transient

† Present address: Technische Thermodynamik, Technische Universität Chemnitz-Zwickau, D09107 Chemnitz, Germany.

‡ Present address: Department of Civil and Systems Engineering, James Cook University, Townsville 4811, Australia.

flows. Wave packets have been observed in the start-up flow of a differentially heated cavity with isothermally heated vertical walls (Patterson & Armfield 1990; Schöpf & Patterson 1995) and in the flow adjacent to a wall subjected to instantaneous heating with a constant-heat-flux boundary condition (Joshi & Gebhart 1987, 1988). The rapid change in the wall boundary condition results in a travelling wave packet as the flow adjusts to new boundary conditions. The wave packet originates at the upstream end of the boundary layer and is amplified as it travels downstream in the flow direction. Finally, self-sustaining oscillations characteristic of an absolute instability have been observed in differentially heated cavities. The oscillations are once again seen in the vertical boundary layers as travelling waves but they do not require external forcing in order to be made visible. The critical Grashof number at which self-sustaining oscillations occur has been ascertained by direct numerical simulations by Le Quéré (1990), Janssen & Henkes (1995) and Paolucci & Chenoweth (1989). The critical Grashof number varies with the cavity geometry, boundary conditions and the Prandtl number.

Hydrodynamic instabilities have been classified as either convective or absolute according to the way in which localized disturbances evolve (Landau & Lifshitz 1959). Consider a localized disturbance introduced into the flow at $x_0$ and at time $t_0$. The criterion for an absolute instability is that, at $x_0$, the disturbance grows for all $t > t_0$. The flow is convectively unstable if the disturbance only grows as it travels away from the source and with signal at $x_0$ decaying. Hence, at any location in a convectively unstable flow, the disturbance is sustained exclusively by the upstream disturbance. If the flow is also spatially evolving, the neutral stability point is then the location where the disturbance changes from decaying with downstream distance to growing with downstream distance. Various flows have been classified as either convectively or absolutely unstable by Huerre & Monkewitz (1990). The existence of wave packets that evolve from isolated disturbances and the downstream amplification of natural disturbances suggest that vertical-plate natural convection flows are convectively unstable for a range of Grashof numbers. In this study we will consider only convectively unstable flows where the Grashof number is below that at which an absolute instability or self-sustaining oscillations occur. Restricting our analysis to convectively unstable flows allows us to examine waves which may be highly unstable but which still behave linearly. This can occur since the amplitude of a convectively unstable wave is completely dependent on the level of the upstream forcing and is not dependent on its local rate of spatial amplification. The behaviour of absolute instabilities is fundamentally different since the amplitude of the disturbance must increase locally until nonlinear effects become important and where linear theory can only be used to predict the critical Grashof number.

The first general formulation of the linear stability problem for natural convection boundary layers by Plapp (1957) was carried out using the parallel base-flow approximation. The resulting normal mode stability equations are similar to the Orr–Sommerfeld equations used in the study of Tollmien–Schlichting waves in forced flows but are modified to include buoyancy forces and coupled with the thermal energy disturbance equation. Parallel linear stability theory has been successful in describing the travelling waves observed in a variety of flow configurations. Many stability analyses have been performed on the steady boundary layer in an unstratified medium (Gebhart *et al.* 1988). In these analyses the frequency that is most highly amplified has matched the experimentally observed frequency. Armfield & Patterson (1992) showed, using a linear stability analysis, that the most amplified wave frequency and velocity matched those seen in a wave packet disturbance observed numerically and

experimentally. However, in these studies the waves were observed downstream of the neutral stability point and the validity of the parallel theory near the neutral point was not tested. An exception to this was the study by Polymeropoulos & Gebhart (1967) where disturbances were artificially imposed on the system. The neutral stability points could then be located and some agreement with parallel linear stability analysis near the neutral stability point could be obtained.

Several previous studies have examined the effect of incorporating non-parallel flow into the stability analysis. In all the flow regimes described the boundary layer is growing and the horizontal velocity allows the boundary layer thickness to change in the downstream direction. Consequently, any wave travelling along the boundary layer must also evolve to account for the boundary layer growth. Haaland & Sparrow (1973) performed non-parallel analysis by a straightforward inclusion of the non-parallel terms in the modified Orr–Sommerfeld equations. However, the proposed waveform remained a plane wave which prevented variation of the waveform in the streamwise direction. More recently, formulations that model the streamwise variations in the eigenfunction have been developed. Wakitani (1985) utilized the WKB method in his formulation to study the stability of a buoyant plume. A similar formulation was used to study a mixed convection boundary layer in Lee, Chen & Armaly (1988). In each case the analysis required the base flow to be described by a similarity solution to the boundary layer equations. A non-parallel formulation proposed by Bertolotti, Herbert & Spalart (1992) has been applied to forced boundary layer flows. By assuming that the perturbation eigenfunction has the same slow variation in the downstream direction as the base flow they were able to formulate parabolized stability equations. The parabolized stability equations (PSE) can not only model the non-parallel effects but can also be extended to include nonlinear and three-dimensional effects.

A different approach to the study of boundary layer stability was developed by Fasel & Konzelmann (1990). Direct numerical simulations of a forced flat-plate boundary layer were performed in which disturbances are imposed on the flow. By forcing disturbances with a range of single frequencies the stability properties of the boundary layer are determined. The method allows all possible non-parallel effects to be ascertained and by imposing small disturbances the resulting travelling waves have a linear form. Recently, a similar approach has been used for flows in a differentially heated cavity (Armfield & Janssen 1996; Janssen & Armfield 1996). The numerical solution to the steady cavity flow was first obtained and then temperature disturbances were imposed by the inclusion of a heat source near the upstream end of the boundary layer.

In this study we use the PSE assumptions to formulate a non-parallel linear stability analysis which we apply to the vertical natural convection boundary layer in a differentially heated cavity. The PSE are solved locally at particular heights up the cavity wall. The results using the PSE are compared to stability analysis using the conventional parallel flow approximations as well as those obtained by full numerical simulation of the waves, referred to here as direct stability analysis. This is the first time simultaneous stability studies have been undertaken for a natural convection boundary layer flow and allows the accuracy of the parallel assumptions to be ascertained and the non-parallel formulation to be tested.

## 2. Non-parallel linear analysis

The parabolized stability equations are now developed for a general buoyancy-driven boundary layer flow adjacent to a heated vertical wall. The governing equations are the two-dimensional Navier–Stokes and energy equations based on the Boussinesq assumptions which, given in terms of the streamfunction, $\tilde{\psi}$, and temperature, $\tilde{T}$, are

$$\left(\frac{\partial}{\partial\tilde{t}}+\frac{\partial\tilde{\psi}}{\partial\tilde{y}}\frac{\partial}{\partial\tilde{x}}-\frac{\partial\tilde{\psi}}{\partial\tilde{x}}\frac{\partial}{\partial\tilde{y}}-\nu\nabla^2\right)\nabla^2\tilde{\psi}-g\beta\tilde{T}_{\tilde{y}}=0, \tag{2.1a}$$

$$\left(\frac{\partial}{\partial\tilde{t}}+\frac{\partial\tilde{\psi}}{\partial\tilde{y}}\frac{\partial}{\partial\tilde{x}}-\frac{\partial\tilde{\psi}}{\partial\tilde{x}}\frac{\partial}{\partial\tilde{y}}-\kappa\nabla^2\right)\tilde{T}=0. \tag{2.1b}$$

Cartesian coordinates are used where $\tilde{x}$ is the vertical or streamwise direction and $\tilde{y}$ is the horizontal or cross-stream direction. The fluid properties are the coefficient of thermal expansion, $\beta$, the kinematic viscosity, $\nu$, and the thermal diffusivity, $\kappa$, and $g$ is the acceleration due to gravity. The equations can be non-dimensionalized with the temperature scale, $\Delta T$, determined from the thermal boundary condition at the wall, the boundary layer thickness, $\delta$, and the velocity scale, $U_b=g\beta\Delta T\delta^2/\nu$. Referring to the non-dimensional base-flow streamfunction and temperature as $(\overline{\psi}(x,y),\overline{T}(x,y))$, and the perturbation as $(\psi'(x,y,t),T'(x,y,t))$, the nonlinear stability equations are formed by substitution of $\psi=\overline{\psi}+\psi'$ and $T=\overline{T}+T'$ into the non-dimensionalized Navier–Stokes and energy equations. The linearized equations are formed by eliminating the nonlinear terms and are given by

$$\begin{aligned}\psi'_{xxt}+\psi'_{yyt}+\psi'_y\overline{\psi}_{xxx}-\psi'_x\overline{\psi}_{xxy}+\psi'_y\overline{\psi}_{yyx}-\psi'_x\overline{\psi}_{yyy}+\psi'_{xxx}\overline{\psi}_y-\psi'_{xxy}\overline{\psi}_x\\ +\psi'_{yyx}\overline{\psi}_y-\psi'_{yyy}\overline{\psi}_x=\frac{1}{Gr_\delta}(\nabla^4\psi'+T'_y),\end{aligned} \tag{2.2a}$$

$$T'_t+T'_x\overline{\psi}_y+\overline{T}_x\psi'_y-T'_y\overline{\psi}_x-\overline{T}_y\psi'_x=\frac{1}{Gr_\delta Pr}(T'_{xx}+T'_{yy}), \tag{2.2b}$$

in which the Prandtl number is defined by $Pr\equiv\nu/\kappa$ and the Grashof number by $Gr_\delta\equiv g\beta\Delta T\delta^3/\nu^2$. Solutions for the perturbations, $(\psi',T')$, are then sought of the form

$$\psi'(x,y,t)=\psi(x,y)\exp\left(\int_{x_0}^{x}k(\xi)\mathrm{d}\xi-\mathrm{i}\omega t\right)+\text{c.c.}, \tag{2.3a}$$

$$T'(x,y,t)=T(x,y)\exp\left(\int_{x_0}^{x}k(\xi)\mathrm{d}\xi-\mathrm{i}\omega t\right)+\text{c.c.}, \tag{2.3b}$$

where c.c. stands for the complex conjugate and $x_0$ is a height above the leading edge of the wall. The perturbation is a two-dimensonal spatially evolving wave with real frequency $\omega$. The first part of the perturbation is a complex eigenfunction, $(\psi(x,y),T(x,y))$, that describes the variation of the waveform in the cross-stream and downstream directions. The other part of the perturbation is an exponential that describes the wave-like nature of the disturbance with $k_r(x)$, the real part of $k(x)$, being the exponential growth rate and the imaginary part of $k(x)$, $k_i(x)$, being the downstream wavenumber.

The base flow is a boundary layer in which the downstream variation is slow and which can be approximated by the solution to the equations with the boundary layer approximation. The boundary layer equations however cannot be used to describe the perturbation since the perturbation wavelengths that are of interest are too short for the second derivatives in the downstream direction to be neglected. The PSE

make use of the observation that, for Tollmien–Schlichting waves, the waveform eigenfunction, the wavelength and the growth rate all vary slowly in the downstream direction. Hence, the equivalent boundary layer approximations can be made for the perturbation eigenfunction. The PSE are then formulated from the perturbation equations (2.2) by neglecting all the base flow and perturbation eigenfunction terms with second- and higher-order $x$ derivatives, as well as multiples of terms each with first- or higher-order $x$ derivatives. Applying these assumptions to the perturbation form (2.3) the derivatives of the perturbation with respect to $x$ can be written as

$$\frac{\partial^m \psi'}{\partial x^m} = \left[k^m \psi + m k^{m-1} \frac{\partial \psi}{\partial x} + \frac{m}{2}(m-1)k^{m-2}\frac{\mathrm{d}k}{\mathrm{d}x}\psi\right] \exp\left(\int_{x_0}^{x} k(\xi)\mathrm{d}\xi - \mathrm{i}\omega t\right) + \text{c.c.}, \tag{2.4a}$$

$$\frac{\partial^m T'}{\partial x^m} = \left[k^m T + m k^{m-1} \frac{\partial T}{\partial x} + \frac{m}{2}(m-1)k^{m-2}\frac{\mathrm{d}k}{\mathrm{d}x}T\right] \exp\left(\int_{x_0}^{x} k(\xi)\mathrm{d}\xi - \mathrm{i}\omega t\right) + \text{c.c.} \tag{2.4b}$$

We also assume that the wavelength and growth rate vary slowly in the downstream direction so that $\mathrm{d}^2k/\mathrm{d}x^2$ and the product of $\mathrm{d}k/\mathrm{d}x$ with other first-order derivatives are negligible. Substituting the perturbation forms from equations (2.4) into the perturbation equations gives,

$$(L_{0,1} + L_{1,1})\psi + L_{0,2}T + L_{2,1}\frac{\partial \psi}{\partial x} + \frac{\mathrm{d}k}{\mathrm{d}x}L_{3,1}\psi = 0, \tag{2.5a}$$

$$(M_{0,1} + M_{1,1})\psi + (M_{0,2} + M_{1,2})T + M_{2,1}\frac{\partial \psi}{\partial x} + M_{2,2}\frac{\partial T}{\partial x} + \frac{\mathrm{d}k}{\mathrm{d}x}M_{3,2}T = 0, \tag{2.5b}$$

with the differential operators,

$$L_{0,1} = -\frac{1}{Gr_\delta}(\mathrm{D}^2 + k^2)^2 + (\overline{\psi}_y k - \mathrm{i}\omega)(\mathrm{D}^2 + k^2) - \overline{\psi}_{yyy}k,$$

$$L_{0,2} = -\frac{1}{Gr_\delta}\mathrm{D}, \quad L_{1,1} = \overline{\psi}_{xyy}\mathrm{D} - \overline{\psi}_x(\mathrm{D}^3 + k^2\mathrm{D}),$$

$$L_{2,1} = -\frac{1}{Gr_\delta}(4k\mathrm{D}^2 + 4k^3) + \overline{\psi}_y(\mathrm{D}^2 + 3k^2) - 2\mathrm{i}k\omega - \overline{\psi}_{yyy},$$

$$L_{3,1} = -\frac{2}{Gr_\delta}(\mathrm{D}^2 + 3k^2) - \mathrm{i}\omega + \overline{\psi}_y 3k,$$

$$M_{0,1} = -\overline{T}_y k, \quad M_{0,2} = -\frac{1}{Gr_\delta Pr}(\mathrm{D}^2 + k^2) - \mathrm{i}\omega + \overline{\psi}_y k,$$

$$M_{1,1} = \overline{T}_x\mathrm{D}, \quad M_{1,2} = -\overline{\psi}_x\mathrm{D}, \quad M_{2,1} = -\overline{T}_y,$$

$$M_{2,2} = -\frac{1}{Gr_\delta Pr}2k + \overline{\psi}_y, \quad M_{3,2} = -\frac{1}{Gr_\delta Pr},$$

in which D refers to differentiation with respect to $y$.

As it stands there is some ambiguity in the partition of the perturbation between its oscillatory and slowly varying components. As discussed in Bertolotti *et al.* (1992) this can be overcome by enforcing a condition which restricts the downstream variation of the eigenfunction. Here, we shall solve the PSE locally at a height $x_0$ where the normalization condition that $k$ is constant is used. Hence we extend the local solution given by equation (26) in Bertolotti *et al.* (1992) to our case of a natural convection

boundary layer. We shall demonstrate *a posteriori* that setting $k$ to a constant in the local solution does restrict the downstream variation in the eigenfunctions as required. In the local solution procedure the base flow and the perturbation eigenfunction are written as a Taylor series expansion about the height $x_0$. The boundary layer approximation made by the PSE ensures that all but the first two terms in the expansion are neglected. With the expansion of the perturbation eigenfunction now written as

$$\psi(x, y, t) = \psi_0(y) + (x - x_0)\psi_1(y), \tag{2.6a}$$

$$T(x, y, t) = T_0(y) + (x - x_0)T_1(y), \tag{2.6b}$$

and the base flow as

$$\overline{\psi}(x, y) = \overline{\psi}((x_0, y) + (x - x_0)\overline{\psi}_x(x_0, y), \tag{2.7a}$$

$$\overline{T}(x, y) = \overline{T}(x_0, y) + (x - x_0)\overline{T}_x(x_0, y), \tag{2.7b}$$

substituting into (2.2) gives the local PSE:

$$L_{0,1}\psi_0 + L_{0,2}T_0 + L_{1,1}\psi_0 + L_{2,1}\psi_1 = 0, \tag{2.8a}$$

$$M_{0,1}\psi_0 + M_{0,2}T_0 + M_{1,1}\psi_0 + M_{1,2}T_0 + M_{2,1}\psi_1 + M_{2,2}T_1 = 0, \tag{2.8b}$$

$$L_{0,1}\psi_1 + L_{0,2}T_1 + L_{4,1}\psi_0 = 0, \tag{2.8c}$$

$$M_{0,1}\psi_1 + M_{0,2}T_1 + M_{4,1}\psi_0 + M_{4,2}T_0 = 0. \tag{2.8d}$$

The additional differential operators are given by

$$L_{4,1} = \overline{\psi}_{xy}(k\mathrm{D}^2 + k^3) - \overline{\psi}_{yyyx}k,$$

$$M_{4,1} = -\overline{T}_{xy}k, \quad M_{4,2} = \overline{\psi}_{xy}k.$$

The base flow fields $(\overline{\psi}, \overline{T})$, are now evaluated at $x = x_0$ and given appropriate boundary conditions, determined by the particular base flow under consideration, the eigenvalue problem can then be solved.

It should be noted that in order to account for the downstream variation in the base flow the perturbation is divided into two functions, both containing $x$. As a result there no longer exists a plane wave solution with a straightforward definition of the wavenumber and spatial amplification as the gradient of the phase. Also, in defining the perturbation this way we have incorporated all of the downstream variation of the wavenumber and amplification into the eigenfunction. The value for $k$ represents only one component of the physical amplification and wavenumbers which we define here as the real and imaginary parts of the downstream gradient of the perturbation, normalized by the perturbation. The amplification and wavenumber further depend on the component of the perturbation taken and, for instance, different values will result for the temperature component verses the velocity components. The physical wavenumbers and amplifications are the sum of two components, one arising from the exponential term and the other from the algebraic $x$ dependence in the eigenfunction. Using the non-parallel formulation the physical amplification, $a_q^S$, and wavenumbers, $k_q^S$, at a height, $x_0$, and for a flow variable, $q$, are defined by

$$a_q^S(x_0, y) \equiv \mathrm{Re}\left(\frac{1}{q'(x_0, y, t)}\frac{\partial}{\partial x}q'(x_0, y, t)\right) = k_r(x_0) + \mathrm{Re}\left(\frac{q_1(x_0, y)}{q_0(x_0, y)}\right), \tag{2.9}$$

$$k_q^S(x_0, y) \equiv \mathrm{Im}\left(\frac{1}{q'(x_0, y, t)}\frac{\partial}{\partial x}q'(x_0, y, t)\right) = k_i(x_0) + \mathrm{Im}\left(\frac{q_1(x_0, y)}{q_0(x_0, y)}\right). \tag{2.10}$$

Note that although the formulation is non-parallel in the sense that the downstream variation in the base flow and perturbations are modelled the solutions are still strictly local in character at the particular $x_0$ chosen.

The PSE reduce to the conventional parallel linear stability equations in the limit of parallel flow. The linear stability equations with parallel flow approximations are formed by assuming a perturbation of the form

$$\psi'(x, y, t) = \psi_0(y)\exp(kx - \mathrm{i}\omega t), \tag{2.11a}$$

$$T'(x, y, t) = T_0(y)\exp(kx - \mathrm{i}\omega t), \tag{2.11b}$$

and the base flow is approximated locally by

$$\overline{\psi}(x, y) = \overline{\psi}(x_0, y), \quad \overline{T}(x, y) = \overline{T}(x_0, y). \tag{2.12a,b}$$

Substituting these into the perturbation equations (2.2) the parallel flow linear stability equations are

$$L_{0,1}\psi_0 + L_{0,2}T_0 = 0, \quad M_{0,1}\psi_0 + M_{0,2}T_0 = 0, \tag{2.13a,b}$$

with the differential operators

$$L_{0,1} = -\frac{1}{Gr_\delta}(\mathrm{D}^2 + k^2)^2 + (\overline{\psi}_y k - \mathrm{i}\omega)(\mathrm{D}^2 + k^2) - \overline{\psi}_{yyy}k, \quad L_{0,2} = -\frac{1}{Gr_\delta}\mathrm{D},$$

$$M_{0,1} = -\overline{T}_y k, \quad M_{0,2} = -\frac{1}{Gr_\delta Pr}(\mathrm{D}^2 + k^2) - \mathrm{i}\omega + \overline{\psi}_y k.$$

## 3. Application to the differentially heated cavity

The parallel and non-parallel linear stability equations developed above are applicable to a range of buoyancy-driven boundary layer flows. Here, they are applied to the steady-state flow in a differentially heated cavity. The base flow used for the linear stability analyses is obtained from the steady-state numerical solution to the cavity problem described below. A direct stability analysis of the same flow is also carried out for comparison to the linear stability results.

The flow configuration is a square cavity of height, $H$, with isothermal vertical sidewalls at temperatures $T_h$ and $T_c$ and adiabatic top and bottom walls. The governing equations are the two-dimensional Navier–Stokes energy equations with the Boussinesq assumptions. A different scaling is applied to the cavity since the problem now has an imposed length scale, $H$. Using the length, velocity and temperature scales, $H$, $\nu/H$ and $\Delta T = (T_h - T_c)/2$ the Navier–Stokes and energy equations form the set of non-dimensional equations

$$U_x + V_y = 0, \tag{3.1a}$$

$$U_t + UU_x + VU_y = -P_x + U_{xx} + U_{yy} + Gr_H T, \tag{3.1b}$$

$$V_t + UV_x + VV_y = -P_y + V_{xx} + V_{yy}, \tag{3.1c}$$

$$T_t + UT_x + VT_y = \frac{1}{Pr}(T_{xx} + T_{yy}) + S. \tag{3.1d}$$

The hot wall is on the left-hand side of the cavity with the origin of the coordinate system at the base of the hot wall and $x$ and $y$ being the vertical and horizontal

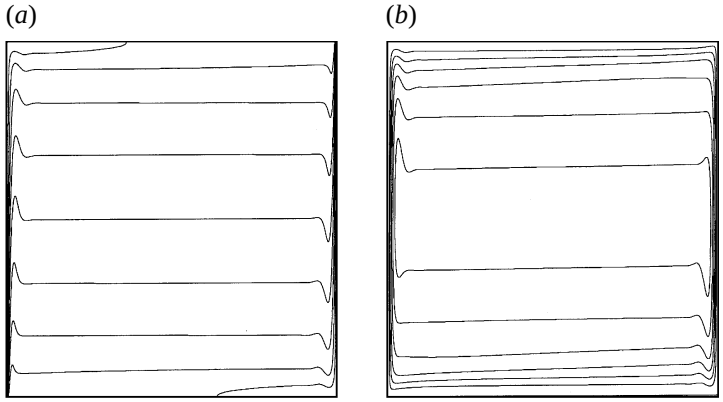


FIGURE 1. (*a*) The temperature field, $\overline{T}$, at steady state: isovalues are $-1.0, (0.2), 1.0$. (*b*) The streamfunction field , $\overline{\psi}$, at steady state: isovalues are $0, (2), 12$.

coordinates respectively. The heat source term, $S$, is zero except when the direct stability analysis is performed. The non-dimensionalized vertical and horizontal velocities are $U$ and $V$ respectively and the values of the non-dimensional parameters are $Gr_H \equiv g\beta\Delta T H^3/\nu^2 = 4 \times 10^7$ and $Pr = 7.5$.

The non-dimensionalized Navier–Stokes equations are solved numerically using an implicit second-order time integration and a finite volume spatial discretization on a non-staggered mesh. The procedure is that described in Patterson & Armfield (1990) and further details are provided in Armfield (1991, 1994). Briefly, the procedure uses second-order central differences to approximate the second derivative, pressure gradient and divergence terms, and the QUICK scheme for the advective terms. Grid refinement tests and the comparison between the direct stability and the non-parallel stability results were used to ensure the solutions were converging to grid and time-step independent results. The calculations displayed were obtained using a 121 by 121 grid discretization and time step of $\Delta t = 5 \times 10^{-7}$. A stretched grid ensured that the vertical boundary layers received the highest resolution. Figure 1 shows the steady-state numerical solution of the temperature and streamfunction fields. The following sections examine the stability of the hot wall only, recognizing that with symmetry the results for the cold wall are identical.

### 3.1. *Linear stability analysis*

For the Grashof/Prandtl number combination chosen the flow converges to a steady solution in which the interior is stratified and thin boundary layers exist adjacent the vertical walls. Henkes & Hoogendoorn (1993) demonstrated the boundary layer character of this flow by calculating numerically the flow using the boundary layer equations. The boundary layer solution matched the full numerical solution for Grashof numbers greater than $10^6$. The boundary layer length and velocity scales are given by $\delta = H/Gr_H^{1/4}$ and $U_b \equiv g\beta\Delta T\delta^2/\nu = Gr_H^{1/2}\nu/H$. Although the flow is absolutely stable according to the definition of Landau & Lifshitz (1959) we shall show that certain regions in the vertical boundary layers are convectively unstable.

At any given height $x_0$ in the cavity the linear stability analysis is performed for a horizontal cross-section of the flow. The base-flow quantities required for the parallel stability calculations are $u(x_0, y), u_{yy}(x_0, y)$ and $T_y(x_0, y)$. These, and the additional base-flow quantities required in the non-parallel analysis, $u_x(x_0, y)$, $u_{yyx}(x_0, y)$, $v(x_0, y)$, $v_{yy}(x_0, y)$, $T_x(x_0, y)$ and $T_{xy}(x_0, y)$, are shown in figure 2 for a height $x_0 = 0.5$. As

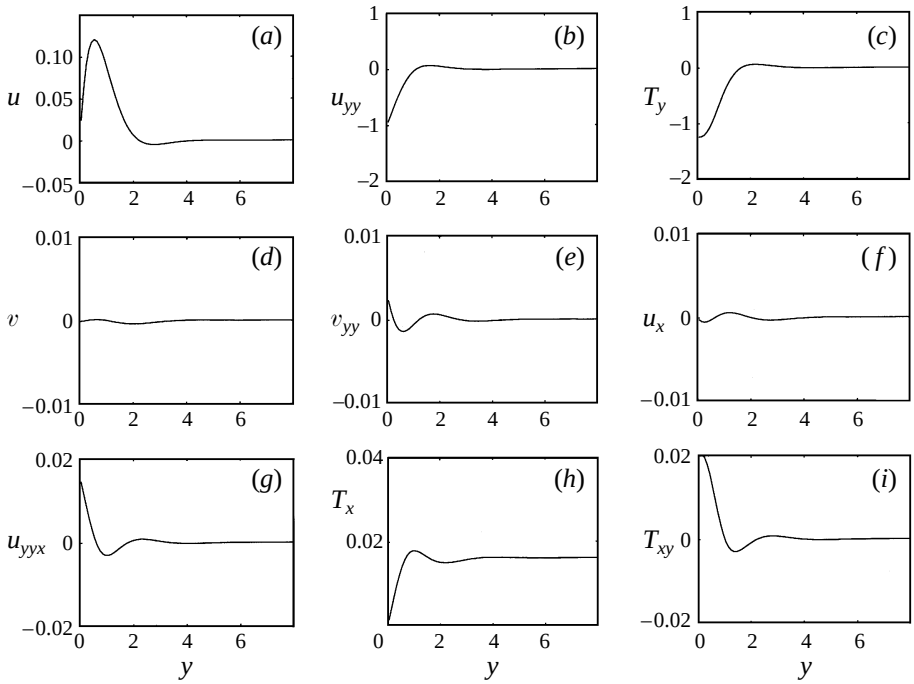


FIGURE 2. The base-flow fields adjacent to the hot wall for $x/H = 0.5$. The fields are scaled with respect to the boundary layer scalings, $\delta$ and $U_b$.

expected for the boundary layer region the base-flow terms that have $x$-derivatives of the base-flow streamfunction and temperature are of $O(Gr_\delta^{-1})$.

Using the parallel analysis, equations (2.13*a,b*) are subject to homogeneous boundary conditions for $\psi_0$, $\psi_{0y}$ and $T_0$ on the hot wall at $y = 0$ and also at the opposite wall, $y = 1$. In the non-parallel formulation equations (2.8) have homogeneous boundary conditions for $\psi_0$, $\psi_{0y}$, $\psi_1$, $\psi_{1y}$, $T_0$ and $T_1$ at $y = 0$ and $y = 1$. For waves travelling upwards in the hot boundary layer the eigenfunctions asymptote to zero well before reaching the cold wall. This allows the location of the outer boundary condition to be chosen at $y = y_{max} < 1$. An appropriate value for $y_{max}$ is chosen such that further increasing $y_{max}$ results in a negligible change in the solution. In the results presented here $y_{max}$ ranges between 0.1 and 0.2.

The stability equations are solved using a straightforward shooting method with orthonormalization (Davey 1973) that simultaneously solves for the eigenfunctions, $\psi_0$, $\psi_1$, $T_0$ and $T_1$ and the complex eigenvalue, $k$, for a given frequency, $\omega$, and height, $x_0$.

### 3.2. *Direct stability analysis*

Direct stability analysis allows the stability properties of individual frequency components to be examined by forcing the flow with a single frequency. Since the solution utilizes the full Navier–Stokes and energy equations all possible non-parallel effects are incorporated in the analysis. The heat source term, which was zero in the development of the steady flow, is used to introduce perturbations into the flow at the base of the hot boundary layer. The source term, $S$, is non-zero only in the region,

$0 < x < 0.01$, $0 < y < 0.01$ where

$$S = A \sin(2\pi f_i t). \tag{3.2}$$

After an initial transient phase, where the disturbance spreads up the boundary layer, a steady pattern of oscillations over the boundary layer is established. The perturbations are rapidly damped once they reach the top boundary and are not carried across to the opposite cold wall. The amplitude of the imposed perturbation, $A$, was chosen such that the resultant wave remained almost linear, which was tested by checking that the maximum amplitude of the perturbation in the boundary layer was proportional to $A$ and the growth rates were independent of the wave amplitude. In most simulations a value of $A = 0.1$ was used.

The relevant wave properties were ascertained by calculating the wave amplitudes from the time series taken after a steady wave pattern had been established. Hence the amplitude for a given flow variable $q$ is defined as

$$A_q(x, y) = \overline{\left(q(x, y, t) - \overline{q(x, y, t)}\right)^2}^{1/2} \tag{3.3}$$

where the overbar refers to the time mean over approximately ten wave periods. The amplification derived from the direct stability analysis is then

$$a_q^D(x, y) = \frac{1}{A_q(x, y)} \frac{\partial}{\partial x} A_q(x, y). \tag{3.4}$$

## 4. Results

Results were obtained for a range of heights up the hot boundary layer and over a range of frequencies. We present results for a selection of frequencies and positions which illustrate features of the travelling waves in a non-parallel flow and the importance of non-parallel assumptions in the stability analysis. The linear stability analysis is discussed with comparison to the benchmark direct stability analysis results.

### 4.1. *Transverse properties*

The complex-valued eigenfunctions that result from the linear stability analysis each comprise a magnitude and a phase component. For example, the temperature eigenfunction, $T_0(y)$, can be written as

$$T_0(y) = |T_0(y)| \exp(\mathrm{i} P_{T_0}(y)), \tag{4.1}$$

where the magnitude, $|T_0|$, and the phase, $P_{T_0}$, are defined by,

$$|T_0(y)| = \left(\mathrm{Re}(T_0(y))^2 + \mathrm{Im}(T_0(y))^2\right)^{1/2},$$

$$P_{T_0}(y) = \tan^{-1}\left(\frac{\mathrm{Im}(T_0(y))}{\mathrm{Re}(T_0(y))}\right).$$

We will first check our assumption that ignoring the first- and higher-order $x$-derivatives of $k(x)$ in the local solution of the PSE does result in solutions in which the eigenfunction has the same slow $x$ variation as the base flow. Figure 3($a$,$b$) shows the normalized magnitudes of the temperature and vertical velocity eigenfunctions for the frequency $f_i = 5 \times 10^3$ and at cavity height $x = 0.5$, obtained using the non-parallel formulation (2.8). As we shall see later, this frequency results in the most rapidly amplified wave at this height. Figure 3($c$,$d$) shows the gradients, $T_1 \equiv (\partial T'/\partial x)(x_0, y)$

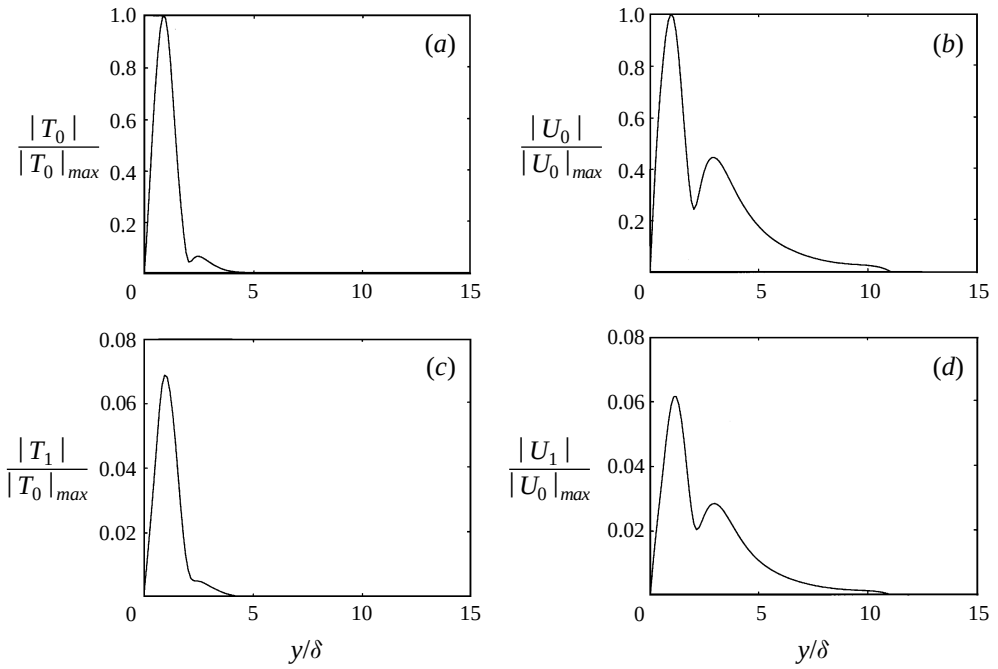


FIGURE 3. (*a*) The normalized magnitude of the temperature eigenfunction, $|T_0|/|T_0|_{max}$ and (*b*) the vertical velocity eigenfunction, $|U_0|/|U_0|_{max}$. (*c*) The temperature eigenfunction gradient $|T_1|/|T_0|_{max}$. (*d*) The vertical velocity eigenfunction gradient $|U_1|/|U_0|_{max}$. All quantities are for frequency $f_i = 5 \times 10^3$ and at height $x = 0.5$.

and $U_1 \equiv (\partial^2\psi'/\partial y \partial x)(x_0, y)$, normalized by the maximums of $T_0$ and $U_0$ respectively. Clearly, $|T_1|/|T_0|_{max}$ and $|U_1|/|U_0|_{max}$ are of the same order as the gradient terms in the base flow, $O(Gr_\delta^{-1})$, as required.

Since the stability analyses is linear, the solutions are valid subject to multiplication by an arbitrary constant. To compare the linear stability analyses to the direct analysis the maximum of the magnitude of the temperature eigenfunction is used to normalize the streamfunction and temperature eigenfunctions. Results from both the linear stability analysis and the direct stability analysis are now presented scaled with respect to the cavity length and velocity scalings, $H$ and $v/H$. The results for the case with $f_i = 5 \times 10^3$ and at height $x = 0.5$ are considered. In figure 4(*a*) the temperature eigenfunctions calculated using parallel and non-parallel theory are shown by the dashed and solid lines respectively and, at this scale, are barely distinguishable. The normalized amplitudes resulting from the direct analysis are shown as open circles. Figure 4(*b*) shows the normalized magnitude of the vertical velocity eigenfunction, $|\psi_{0y}|$. The eigenfunctions in each case match the full numerical results very well. Consider now the spatial growth rates in the downstream direction of the temperature and vertical velocity signals. Using parallel assumptions the amplification, $k_r$, is independent of cross-stream position and flow variable and is shown by the dashed lines in figure 4(*c*,*d*). Using the non-parallel analysis the amplification is dependent on the transverse direction as given by equation (2.9). The variation in amplification across the boundary layer allows the shape of the eigenfunction to change with the flow as it converges or diverges. The non-parallel amplifications are shown in figure 4(*c*,*d*) for the temperature and vertical velocity

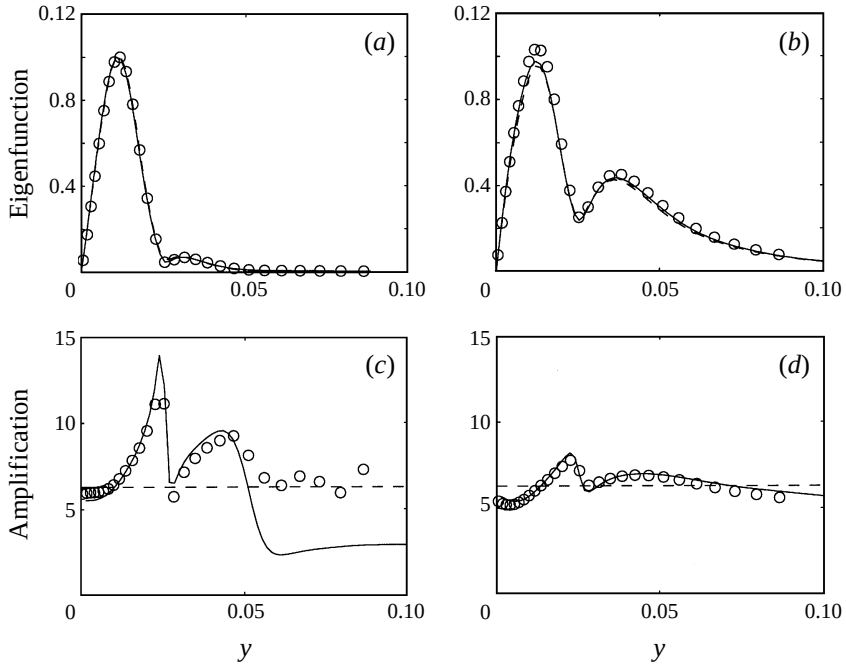


FIGURE 4. (*a*) The temperature eigenfunction, $T_0(x = 0.5, y)$ using non-parallel (solid line) and parallel (dashed line) assumptions and the direct eigenfunction $A_T(x = 0.5, y)$ (circles). (*b*) As for (*a*) but for the vertical velocity eigenfunctions, $\psi_{0y}(x = 0.5, y)$ and $A_U(x = 0.5, y)$. (*c*) The amplifications, $a_T^S(x = 0.5, y)$ (solid line), $k_r(x = 0.5)$ (dashed line) and $a_T^D(x = 0.5, y)$ (circles). (*d*) The amplifications, $a_U^S(x = 0.5, y)$ (solid line), $k_r(x = 0.5)$ (dashed line) and $a_U^D(x = 0.5, y)$ (circles). All quantities are for frequency $f_i = 5 \times 10^3$.

signals respectively and are represented as solid lines. Amplifications calculated from the direct stability analyses, equation (3.4), are shown by the open circles. Clearly the amplification has a strong transverse dependency that cannot be modelled using the conventional parallel theory. It is notable that the transverse dependency is strong despite the fact that at this height the maximum of the transverse velocity is only 0.25% the maximum of the vertical velocity. The non-parallel analysis does however predict the amplification accurately. Disagreement in the temperature amplification for $y > 0.05$, in figure 4(*c*), is not significant as the eigenfunction magnitude is almost zero at these locations.

Shown in figure 5(*a–c*) are the temperature eigenfunctions for a lower frequency, $f_i = 3 \times 10^3$, at three heights, $x = 0.3, 0.5$ and 0.7. The parallel and non-parallel stability results both give good predictions of the eigenfunction seen in the full simulation. The eigenfunctions consist of two peaks with the maximum of each peak shifting further out from the wall with increasing distance up the wall. The size of the outer or second peak is also increasing relative to the size of first inner peak. This behaviour is consistent with the shape of the amplification curves shown in figure 5(*d–f*). The amplification increases across the first peak, then there is a sharp drop in the amplification which is consistent with the eigenfunction peaks moving out from the boundary. The amplification is also higher at the maximum of the second peak than at the first, leading to an increase in the size of the second peak relative to the first.

The prediction of the wavenumber has also been investigated. The non-parallel

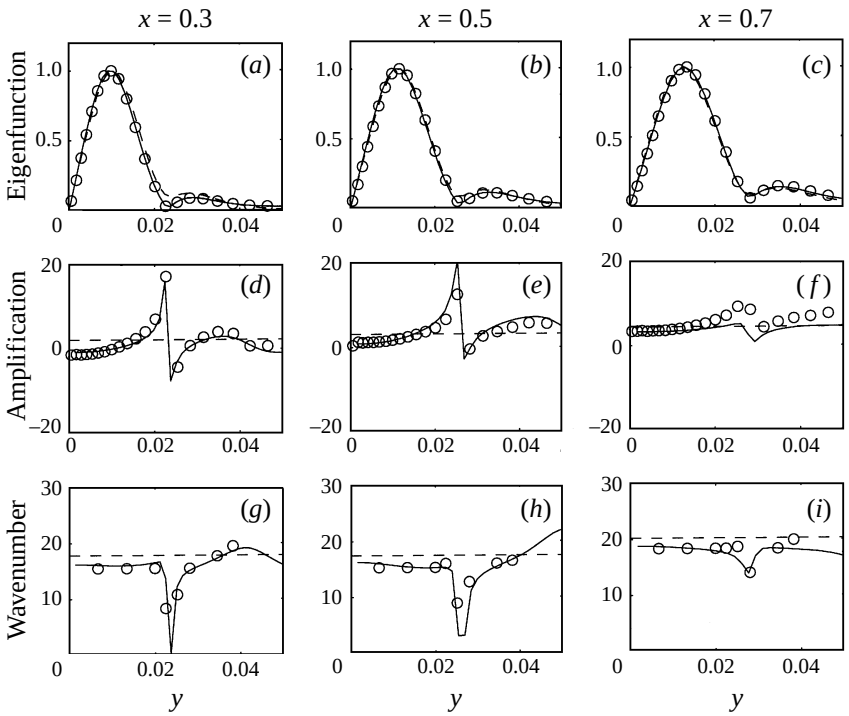


FIGURE 5. The temperature eigenfunction, $T_0$, using non-parallel (solid line) and parallel (dashed line) assumptions and the direct eigenfunction $A_T$ (circles) at $x = 0.3$ ($a$), $x = 0.5$ ($b$) and $x = 0.7$ ($c$). The amplifications, $a_T^S$ (solid line), $k_r$ (dashed line) and $a_T^D$ (circles) at $x = 0.3$ ($d$), $x = 0.5$ ($e$) and $x = 0.7$ ($f$). The wavenumbers, $k_T^S$ (solid line), $k_i$ (dashed line) and $k_T^D$ (circles) at $x = 0.3$ ($g$), $x = 0.5$ ($h$) and $x = 0.7$ ($i$). All quantities are for the frequency $f_i = 3 \times 10^3$.

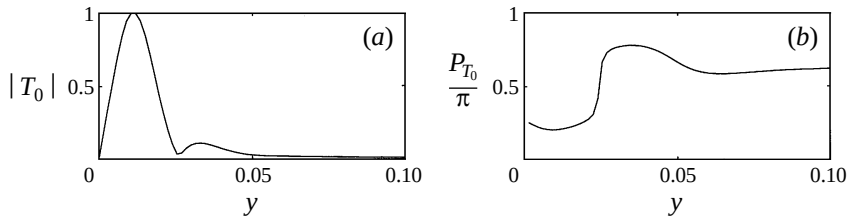


FIGURE 6. ($a$) The magnitude, $|T_0(y)|$, and ($b$) the phase, $P_{T_0}(y)$, of the temperature eigenfunction for $f_i = 3 \times 10^3$ and $x = 0.5$.

analysis predicts that the wavenumber depends on the transverse coordinate as given by equation (2.10). This dependence arises from changes in the phase lag of the disturbance across the boundary layer. The wavenumber, $k_p^D$, is estimated by measuring the peak-to-peak distance in the direct stability analysis. Figure 5($g$–$i$) shows that the parallel analysis overpredicts the wavenumber at each height. At the location of the maximum of the temperature amplitude the wavenumber from the parallel analysis is in error by approximately 10%. Figure 6 shows the magnitude and the phase of the temperature eigenfunction for $f_i = 3 \times 10^3$ and height $x = 0.5$. The minimum in the wavenumber that occurs near $y = 0.025$ results from the 180° phase shift that exists between the inner and outer peaks seen in figure 6. The non-parallel formulation is very successful in predicting this behaviour.

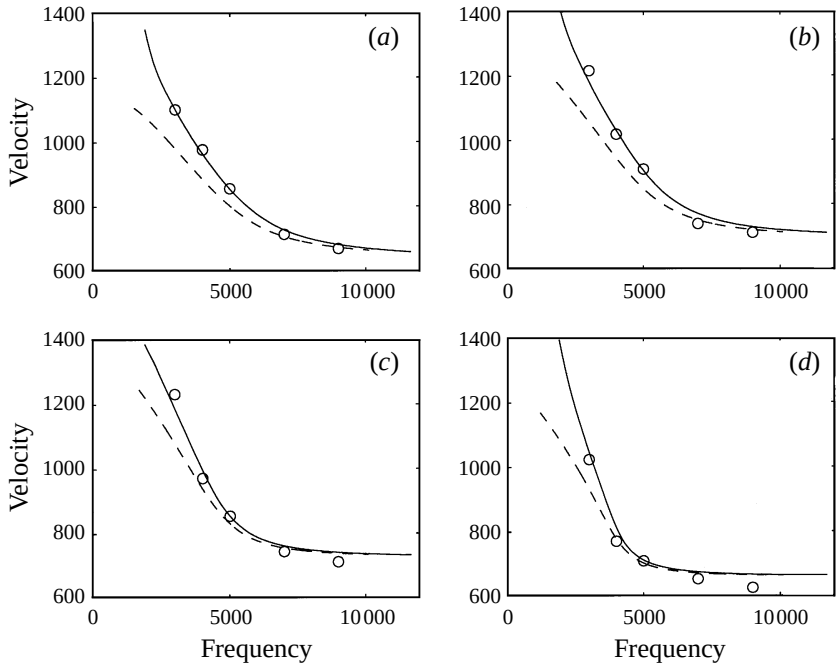


FIGURE 7. The phase velocities, $\omega/k_T^S(y = 0.008)$ (solid line), $\omega/k_T^D(y = 0.008)$ (circles) and $\omega/k_i$ (dashed line) at heights (*a*) $x = 0.2$, (*b*) $x = 0.3$, (*c*) $x = 0.5$ and (*d*) $x = 0.7$.

The phase velocities, $\omega/k_i$, $\omega/k_T^S$ and $\omega/k_T^D$, have also been compared over a range of frequencies. Although the phase velocity does vary across the boundary layer, there is only a weak dependency over the region closest to the wall. A representative transverse distance of $y = 0.008$ is chosen at which to compare the phase velocity of the waves at different heights and frequencies. In figure 7 the phase velocities calculated from the direct stability analysis at heights $x_0 = 0.2, 0.3, 0.5$ and 0.7 are compared to the linear stability results. While the non-parallel theory performs well at all frequencies the agreement between the parallel theory and the direct stability analysis deteriorates as the frequency is decreased.

### 4.2. *Integral properties*

The amplification, at a given height, can be separated into the sum of two parts, the first being the net amplification of the disturbance at the given height, the second redistributing the disturbance across the boundary layer but contributing zero net amplification. In evaluating the parallel and non-parallel theories it is important to ascertain whether the parallel theory predicts the net amplification correctly, despite failing to account for cross-stream variations in the amplification. The integral of the temperature eigenfunction across the boundary layer is used to define the net disturbance amplitude at a given height from which the net amplification can then be calculated. Using the non-parallel analysis the net amplification is then

$$a^S(x) = \mathrm{Re}\left(\frac{1}{\int T'(x,y,t)\mathrm{d}y}\frac{\partial\int T'(x,y,t)\mathrm{d}y}{\partial x}\right) = \frac{1}{\int|T_0(x,y)|\mathrm{d}y}\int a_T^S(x,y)|T_0(x,y)|\mathrm{d}y, \tag{4.2}$$

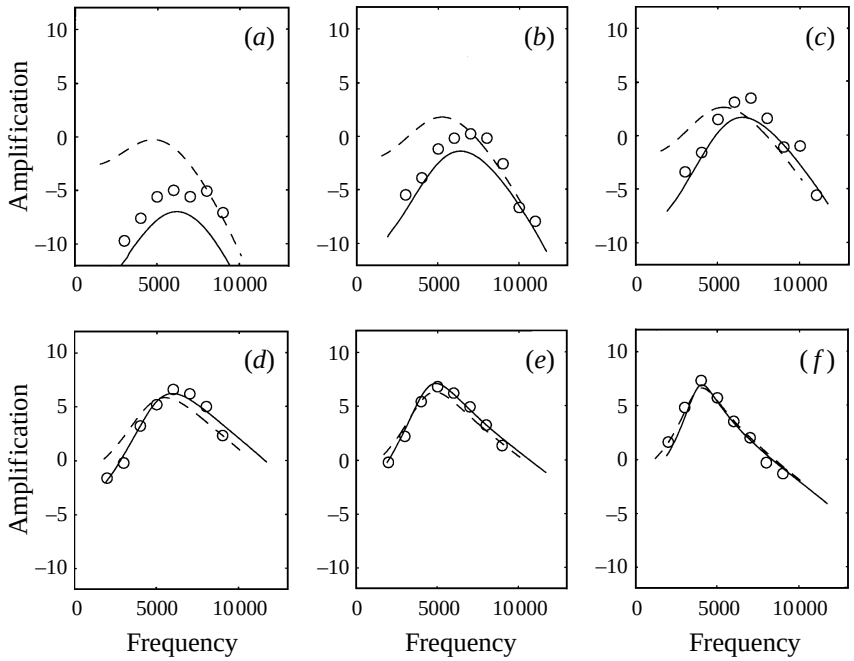


FIGURE 8. The net amplifications, $a^S$ (solid line), $a^D$ (circles) and $k_r$ (dashed line) at heights (*a*) $x = 0.06$, (*b*) $x = 0.08$, (*c*) $x = 0.10$, (*d*) $x = 0.3$, (*e*) $x = 0.5$ and (*f*) $x = 0.7$.

and the equivalent net amplification derived from the direct stability analysis is

$$a^D(x) = \frac{1}{\int A_T(x,y)\mathrm{d}y} \frac{\partial \int A_T(x,y)\mathrm{d}y}{\partial x}. \tag{4.3}$$

Shown in figure 8(*a–c*) are the net amplifications over a range of frequencies and at heights $x = 0.06, 0.08$ and 0.1 which are near the location of the neutral stability point. Figure 8(*b*) shows that the direct stability analysis gives a critical height and frequency of approximately 0.08 and $7 \times 10^3$ respectively. The parallel theory predicts that the flow is more unstable with the critical height near $x = 0.06$ and at a frequency of $5 \times 10^3$. The non-parallel analysis gives a much better prediction of the critical height and frequency. It is also observed that the error in the parallel theory is greater for lower frequencies. The comparison using the integral quantities of other variables, such as the integrated vertical velocity perturbation, give similar results. Figure 8(*d–f*) shows that further up the cavity, at $x = 0.3$, 0.5 and 0.7, the parallel theory provides better predictions and at $x = 0.7$ the parallel theory performs equally as well as the non-parallel formulation. The most amplified frequency decreases with height up the cavity and at $x = 0.7$ it has dropped to $4 \times 10^3$ from $7 \times 10^3$ at the critical point.

## 5. Conclusions

The stability of the vertical boundary layer in a differentially heated cavity at Grashof number $4 \times 10^7$ and Prandtl number 7.5 has been investigated using three different techniques. The first is a linear stability analysis of the flow performed with a local approximation of parallel flow. In the second a local solution of the parabolized

stability equations is used. The PSE formulation is applicable to any slowly varying buoyancy-driven flow adjacent to a vertical wall. Finally a direct stability analysis was performed by introducing small-amplitude sinusoidal disturbances into a numerical simulation of the flow. This allowed the evolution of linear disturbances to be directly calculated with all non-parallel effects incorporated.

Many previously unrecognized features of the stability of non-parallel flow in a cavity have been revealed using the direct stability analysis. The perturbation amplifications and wavelengths exhibit a strong cross-stream dependency. Furthermore, the wave properties also depend on the flow variable considered. The non-parallel formulation for the linear stability equations has resulted in excellent agreement with the direct stability results, both in terms of the amplification and the wavenumber. The parallel formulation for the linear stability analysis does not model the strong cross-stream dependence in the spatial amplification and hence cannot be compared with experimentally determined amplifications from fixed cross-stream locations. In previous numerical and experimental studies the strong transverse dependency has not been recognized and amplifications, based only on a single measurement made at the eigenfunction maximum, matching the parallel theory results may have been fortuitous.

The integral of the temperature perturbation across the boundary layer was used to define a net amplification at any given height up the cavity. At cavity heights where the transverse flow was weak the differences between the parallel and the direct analyses values for the net amplification were small. However, the parallel flow analysis results deteriorated when the transverse flow was increased as was the case near the critical stability point. Hence the parallel analysis underpredicted the critical height and frequency. The parallel analysis also performs poorly at low frequencies. This is not unexpected since the lower frequencies correspond to wavelengths which are longer when compared to the length scale over which streamwise variation in the base flow is occurring.

The frequency of the most amplified wave decreased with height up the cavity. This is in contrast to linear stability results for open non-stratified flows (Gebhart *et al.* 1988) where the most amplified frequency remains relatively constant with downstream distance and a narrow band of frequencies dominates the disturbance response.

## REFERENCES

Armfield, S. W. 1991 Finite difference solutions of the Navier–Stokes equations on staggered and non-staggered grids. *Computers Fluids* **20**, 1–17.

Armfield, S. W. 1994 Ellipticity, accuracy and convergence of the discrete Navier–Stokes equations on staggered and non-staggered grids. *J. Comput. Phys.* **114**, 176–184.

Armfield, S. W. & Janssen, R. J. A. 1996 A direct boundary-layer stability analysis of steady-state cavity convection flow. *J. Heat Fluid Flow* **17**, 539–546.

Armfield, S. W. & Patterson, J. C. 1992 Wave properties of natural convection boundary layers. *J. Fluid Mech.* **239**, 195–212.

Bertolotti, F. P., Herbert, Th. & Spalart, P. R. 1992 Linear and nonlinear stability of the Blasius boundary layer. *J. Fluid Mech.* **242**, 441–474.

Davey, A. 1973 A simple numerical method for solving Orr–Sommerfeld problems. *Q. J. Mech. Appl. Maths* **26**, 401–411.

Fasel, H. & Konzelmann, U. 1990 Non-parallel stability of a flat-plate boundary layer using the complete Navier–Stokes equations. *J. Fluid Mech.* **221**, 311–347.

Gebhart, B., Jaluria, Y., Mahajan, R. L. & Sammakia, B. 1988 *Buoyancy-Induced Flows and Transport*. Hemisphere.

Haaland, S. E. & Sparrow, E. M. 1973 Stability of buoyant boundary layers and plumes taking account of the non-parallelism of the basic flows. *Trans. ASME J. Heat Transfer* **95**, 295–301.

Henkes, R. A. W. M. & Hoogendoorn, C. J. 1993 Scaling of the laminar natural-convection flow in a heated square cavity. *Int. J. Heat Mass Transfer* **36**, 2913–2925.

Huerre, P. & Monkewitz, P. A. 1990 Local and global instabilities in spatially developing flows. *Ann. Rev. Fluid Mech.* **22**, 473–537.

Janssen, R. J. A. & Armfield, S. W. 1996 Stability properties of the vertical boundary layers in differentially heated cavities. *J. Heat Fluid Flow* **17**, 547–556.

Janssen, R. J. A. & Henkes, R. A. W. M. 1995 Influence of Prandtl number on stability mechanisms and transition in a differentially heated square cavity. *J. Fluid Mech.* **290**, 319–344.

Joshi, Y. & Gebhart, B. 1987 Transition of transient vertical natural-convection flows in water. *J. Fluid Mech.* **179**, 407–438.

Joshi, Y. & Gebhart, B. 1988 Transient response of a steady vertical flow subject to a change in surface heating rate. *Intl J. Heat Mass Transfer* **31**, 743–757.

Landau, L. D. & Lifshitz, E. M. 1959 *Fluid Mechanics, Vol. 6 of a Course in Theoretical Physics.* London: Pergamon.

Le Quéré, P. 1990 Transition to unsteady natural convection in a tall water-filled cavity. *Phys. Fluids* A **2**, 503–515.

Lee, S. L., Chen, T. S. & Armaly, B. F. 1988 Non-parallel wave instability of mixed convection flow on inclined flat plates. *Intl J. Heat Mass Transfer* **31**, 1385–1398.

Paolucci, S. & Chenoweth, D. R. 1989 Transition to chaos in a differentially heated vertical cavity. *J. Fluid Mech.* **201**, 379–410.

Patterson, J. C. & Armfield, S. W. 1990 Transient features of natural convection in a cavity. *J. Fluid Mech.* **219**, 469–497.

Plapp, J. E. 1957 The analytic study of the laminar boundary layer stability in free convection. *J. Aero. Sci.* **24**, 318–319.

Polymeropoulos, C. E. & Gebhart, B. 1967 Incipient instability in free convection laminar boundary layers. *J. Fluid Mech.* **30**, 225–240.

Schöpf, W. & Patterson, J. C. 1995 Natural convection in a side-heated cavity: visualization of the initial flow features. *J. Fluid Mech.* **295**, 357–379.

Szewczyk, A. A. 1962 Stability and transition of the free-convection layer along a vertical flat plate. *Intl J. Heat Mass Transfer* **5**, 903–914.

Wakitani, S. 1985 Non-parallel-flow stability of a two-dimensional buoyant plume. *J. Fluid Mech.* **159**, 241–258.